Ratchet based ion pumps for selective ion separations

Alon Herman
Tel Aviv University
Joel Ager III
Lawrence Berkeley National Laboratory https://orcid.org/0000-0001-9334-9751
Shane Ardo
UC Irvine
Gideon Segev (gideons1@tauex.tau.ac.il)
Tel Aviv University https://orcid.org/0000-0002-6175-3458

Article

Keywords:

Posted Date: May 6th, 2022

DOI: https://doi.org/10.21203/rs.3.rs-1538622/v1

Ratchet based ion pumps for selective ion separations

Alon Herman[1], Joel W. Ager[2,3], Shane Ardo[4], and Gideon Segev[1*]

[1]School of Electrical Engineering, Tel Aviv University, 6997801, Israel

[2]Department of Materials Science and Engineering, University of California at Berkeley, Berkeley, CA, 94720, USA

[3]Materials Sciences Division, Lawrence Berkeley National Laboratory, Berkeley, CA, 94720, USA

[4]Department of Chemistry, Department of Chemical & Biomolecular Engineering, Department of Materials Science & Engineering, University of California Irvine, Irvine, CA USA

[*]email: gideons1@tauex.tau.ac.il

ABSTRACT

The development of a selective, membrane-based ion separation technology may prove useful in a wide range of applications such as water treatment, battery recycling, ion specific chemical sensors, extraction of valuable metals from sea water, and bio-medical devices. In this work we show that a flashing ratchet mechanism can be used for high precision ion separation. The suggested ratchet-based ion pumps utilize a unique feature of ratchets, the frequency dependent current reversals, to drive ions with the same charge but different diffusion coefficients in opposite directions. We show that ions with a relative diffusion coefficient difference as small as 1% can be separated by driving them in opposite directions with a velocity difference as high as 1.2 mm/s. Since the pumping properties of the ratchet are determined by an electric input signal, the proposed ion pumps can pave the way for simple large-scale, fit-to-purpose selective ion separation systems.

In recent years there has been a growing demand for membranes capable of extracting a single solute from water.[1–3] The introduction of a highly selective ion separation technology could drive a dramatic progress in a range of applications such as water treatment, resource extraction from sea water, bio memetic systems, and chemical sensors. For example, according to the World Health Organization, the acceptable concentration of lead in drinking water is in the order of several particles per billion[4], and the concentration of NaCl in drinking water is slightly lower than one particle per thousand. Thus, a water decontamination system based on driving ions through a medium with a solute-dependent permeability should be about six orders of magnitudes more permeable to lead than towards sodium ions.

One of the main approaches pursued for solute-solute selective separation is filtration with sub-nanometer pore membranes. In these membranes, the pore diameter is engineered to be between the diameter of the hydrated target ion and its diameter when it is partially dehydrated. Ion transport

through the membrane is achieved by applying energy to partially (or fully) dehydrate ions and transport them through the membrane. Selectivity originates from the difference in the hydration energy between ions and the difference in their transport properties within the pores.[1,2] Despite achieving some success, highly selective separation of same-charge ions remains a fundamental challenge.[1,2] Furthermore, since these membranes rely on functionalized pores with a precise diameter below 1 nm, upscaling these membranes is a great challenge. Moreover, as the membrane selectivity is derived by the pore geometry and chemistry, unique membranes must be designed for every target ion.[2] Another approach for monovalent ion separation is based on the diffusion coefficient dependent response of ions to a pressure induced streaming potential.[1,5–9] However, only a few studies have demonstrated this mechanism and so far their reported selectivity is limited. In this work we propose to use a flashing ratchet mechanism to separate ions with the same charge number according to their diffusion coefficients. Since the selectivity is controlled by the ratcheting process, it does not require energy intensive ion dehydration or complex sub-nanometer structures.

Flashing Ratchets

Electronic flashing ratchets are non-equilibrium devices that utilize modulation of a spatially asymmetric electric field to drive a steady state particle flux.[10–12] Similar to a MOSFET transistor, most of the demonstrated flashing ratchets are comprised of gating electrodes that generate a modulated electric field, and source and drain electrodes between which the ratchet output current flows. The symmetry breaking required to produce a directed current is achieved by structuring the gating electrodes,[13–17] introducing a nonlinear, diode like conductance between the source and drain,[18,19] or by applying different signals to different sets of gating electrodes.[20–26] Fig. 1a shows a schematic illustration of the operating principles of a flashing ratchet driving positive charge.[13,27] The empty circles represent the ions position at the beginning of every step, and the filled circles represent their position at the end of every step. The potential distribution through the device (*V,* solid blue line) is switched between two saw-tooth potential distributions, V^+ and V^-, where $V^- = \alpha V^+$, and the potential asymmetry factor α is negative. Initially the particles rest at the potential minima, for example at x_1. When the potential is switched to V^- at $t = t_0$, the particles drift in both directions. The length of the time interval between t_0 and t_1 is tuned to allow some drifting particles to reach the potential minimum on their right, x_1', but not the potential minimum to their left, x_0'. Hence, when the potential is switched to V^+ at $t = t_1$, some of the particles at x_1' drift further to the right towards x_2, but all the other particles return to their initial position at x_1 resulting in a net current to the right. The asymmetric potential distribution allows some particles to reach the potential minima in one direction before particles drifting in the opposite direction, thus making it essential for a non-zero net current. Fig. 1b illustrates the operation of the same ratchet driving negatively charged particles. Here particles

drift towards the potential peaks and as a result, the same potential distribution and input signal generate a net particle flux in the opposite direction.

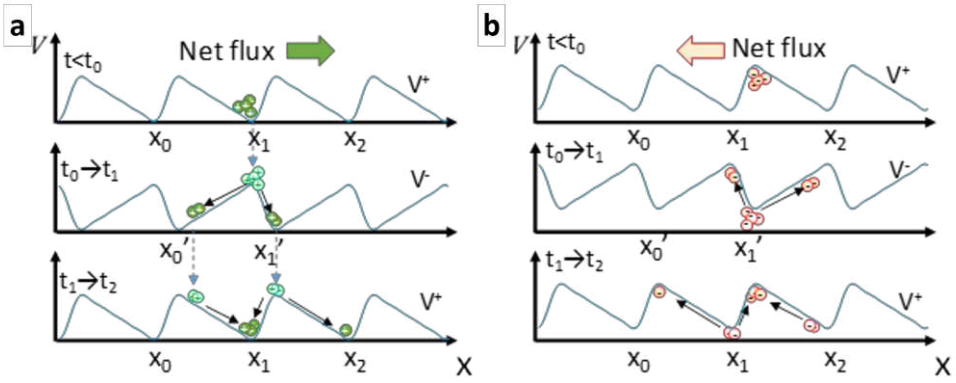

Fig. 1 | The operating principles of a flashing ratchet. a,b, An illustration of a flashing ratchet driving positively charged **(a)** and negatively charged particles **(b)**. The solid blue line illustrates the potential distribution during sequential steps, empty circles mark the position of particles at the beginning of every step and filled circles mark their position at the end of every step.

While in most prior studies flashing rachets were used to drive electrons or holes in semiconductors,[13,14,23–26,15–22] the application of flashing ratchets for ion pumping was only suggested recently. Membranes with oscillating pores for resonant osmosis were theoretically analyzed in terms of ratchet driven transport[28,29] and nanofluidic charge coupled devices, which can be viewed as reversible ratchets,[30] were studied for DNA separations.[31] In prior work, we have utilized these ratcheting principles to demonstrate experimentally a first-of-its-kind ratchet-based ion pump.[32] In all prior analyses of ratchet based ion pumps (RBIPs) for ion separation,[28,29,31] selectivity is achieved by transporting particles with different velocities (in the same direction) according to their diffusion coefficients. However, as discussed above, this approach has a limited selectivity making it unfit for removing trace amounts of ions from solutions.

An important hallmark of ratchets is the ability to invert the direction of particle flow with a change in the input signal frequency.[13,33] The stopping frequency, which is the input signal frequency at which the particle flux changes its direction, is determined by the potential distribution and particles transport properties.[34–36] As a result, for a given ratchet, there can be a frequency at which particles with the same charge but different diffusion coefficients are transported in opposite directions. This effect has been used to sort gold nanoparticles of different sizes and shapes[35–37] and was studied theoretically in ratchets based on pulsating the spacing between the walls of asymmetric periodic channels or their relative position.[38–42] However, this concept has not been applied to ion separations. Here we show that by utilizing velocity reversal in ratchet systems, ions with the same charge can be driven in opposite directions according to their diffusion coefficients. This enables extraction of ions with extremely low relative concentrations if their diffusion coefficient is even slightly different from the main ions in the solution. Since the direction of ion transport is determined by the input signal

frequency, the sorting properties can be tuned in real time providing a simple fit-to-purpose solution for a variety of ion separations applications.

Analysis

In the absence of bulk chemical reactions, the transport of noninteracting ions in a solution is determined by the continuity equation:

$$\frac{\partial C(x,t)}{\partial t} = -\frac{\partial}{\partial x} N(x,t) \tag{1}$$

where $C(x,t)$ is the ion concentration, and $N(x,t)$ is the ion flux. When convection is negligible, the ion flux is driven by drift and diffusion processes:

$$N(x,t) = -D\left[z\beta C(x,t)\frac{\partial}{\partial x}\, U(x,t) + \frac{\partial}{\partial x} C(x,t)\right] \tag{2}$$

Here D is the ion diffusion coefficient, z is the ion charge number, $\beta = e/k_B T_r$ is the inverse thermal voltage, k_B is the Boltzmann constant, T_r is the temperature, and e is the elementary charge. The potential distribution in the system $U(x,t)$ is described as the product of spatial and temporal components:

$$U(x,t) = V(x)g(t) \tag{3}$$

We address in this paper a simple ratchet system that has an infinitely periodic sawtooth distribution in space, with a spatial period L, and is driven by a periodic square wave signal at frequency f. The spatial and temporal contributions are shown in Fig. 2a, and are mathematically described by:

$$V(x) = \begin{cases} V_{max}\dfrac{x/L}{x_c}, & 0 < \dfrac{x}{L} < x_c \\ V_{max}\dfrac{(1-x/L)}{(1-x_c)}, & x_c < \dfrac{x}{L} < 1 \end{cases} \quad ; \quad g(t) = \begin{cases} 1, & 0 < t < \delta \cdot T \\ \alpha, & \delta \cdot T < t < T \end{cases} \tag{4}$$

Where V_{max} is the potential amplitude, and x_c is a measure of the spatial symmetry of the sawtooth, defined as the relative length of the first linear section of the sawtooth potential (see Fig. 2). The temporal modulation $g(t)$ is described by a duty-cycle $\delta = t^+/T$, which is the ratio between the time-duration of the first step, where the potential is at its maximum value, to the total period $T(= 1/f)$. Each time-period is completed with a second step, in which the sawtooth distribution is multiplied by a potential symmetry factor in the range $-1 \leq \alpha \leq 0$.

The continuity equation with periodic boundary conditions was solved numerically. More details on the simulation can be found in the methods section. Our analysis is presented in terms of ion velocity (and not flux), since it is independent of the reference concentration, and therefore is a more general characteristic of the ratchet. We define the net ion velocity, v_{net}, to be the average velocity in space and time:

$$v_{net} = \frac{1}{c_0}\int_0^T \int_0^L \frac{N(x,\tau)}{TL}\, dx\, d\tau \tag{5}$$

Here, the time $\tau = 0$ is defined to be the time at which the system enters its steady-state and the initial state of the system no longer affects its operation.

Since the electric potential distribution is an input in the presented model, and Poisson's equation is not solved; the model does not consider the interactions between the ions, the potential being screened by them, nor the columbic forces arising when separating cations and anions. Such linear sawtooth potential distributions can be obtained in extremely dilute solutions or in devices with a length scale that is smaller than the Debye length. For systems that do not comply with these assumptions the coupled Nernst-Poisson-Planck equations would need to be solved. Thus, the model presented here offers an ideal testcase that can help determine the optimal electric potential distribution for a given application.

Velocity reversal

Ratchets can be useful for many applications, but of particular interest to us is to examine the range of parameters that drive ions with the same charge (polarity and valence), in opposite directions. The ion response to a ratchet drive was found by calculating the net ion velocity, v_{net}, for various input signals, $g(t)$, potential distributions, $V(x)$, and ions with diffusion coefficients, D. Unless stated otherwise, the ratchet parameters that are used in the analysis are: $L = 1$ µm, $x_c = 0.7$, $V_{max} = 2.5$ V, $\beta = 39.59\ \mathrm{V}^{-1}$, $\delta = 0.25$, $\alpha = -0.5$, the ion charge number is $z = 1$, and the reference concentration is $c_0 = 1\ \mathrm{mol/m^3}$. Fig. 2b illustrates a typical velocity reversal example. The figure shows the net ion velocity as a function of the ratchet signal frequency for two ions with different diffusion coefficients. For input signal frequencies between 62–103 kHz, the low D ions have a positive net velocity, and the high D ions have a negative net velocity.

When the ratchet is operated at $f = 83$ kHz, the difference in net velocities is the largest. The variation of the average ion velocity along a time-period is analysed in the SI and shown in Supplementary Fig. 2. Fig. 2c and Fig. 2d show the distribution of the low D and high D ions respectively, at a few key times along a time-period when the ratchet is operated at $f = 83$ kHz. Starting from $\tau = 0$, the entire ion population is crowded around the potential minima. After the first potential switch at $\tau = 0.02T$, the ion population is split into two groups drifting in opposite directions. By the time $\tau = 0.25T$, nearly all the high D ions have reached the new potential minima, while the majority of the low D ions have not. After the second potential switch, at $\tau = 0.26T$, the ions split again, but since the electric fields are lower ($\alpha = -0.5$), the groups drift apart more slowly. This allows more ions to diffuse over the potential peak and join the ions drifting in the negative x direction. When the groups are completely separated, at $\tau = 0.28T$, this process stops. The overall effect is a transfer of ions from the low field side of the sawtooth to the high field side, a phenomenon we term *injection*. An approximation of the net velocity can be made by noticing that 57% of the high D ions are traveling to the left after the first potential switch, while after the second switch only 45%

return. Hence, in every time-period, about 12% of the ions are moving one spatial period in the negative direction, resulting in a net velocity of $v_{net} \approx -12\% \cdot L/T = -1$ cm/s. For the low D ions however, only a fraction of the ions reaches the potential minimum before the second potential switch. As a result, the injection from right to left ($\tau = 0.28T$) is less significant, and while 60% of the ions are traveling to the left after the first potential switch, 75% return after the second switch, yielding a positive net velocity of about $v_{net} \approx 15\% \cdot L/T = 1.25$ cm/s.

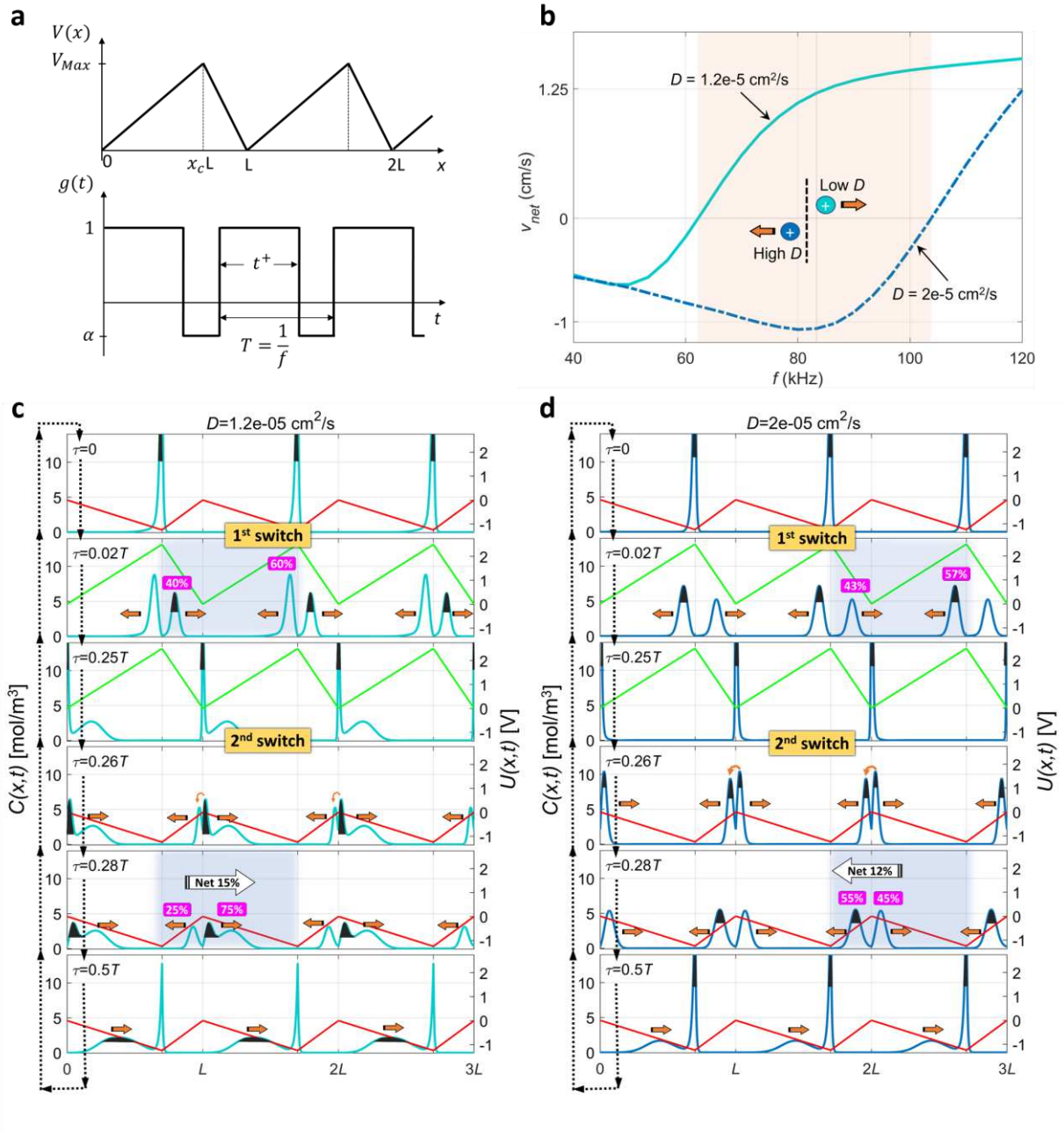

Fig. 2 | Potential distribution and velocity reversal mechanism. a, The spatial and temporal components of the potential distribution. **b**, The net velocity of two positively charged monovalent ions ($z = 1$), as a function of the input signal frequency. In the shaded region the ions move in opposite directions. **c**,**d**, The concentration response $C(x,t)$ of two positively charged monovalent ions ($z = 1$) with diffusion coefficients $D = 1.2 \cdot 10^{-5}\ cm^2/s$ (**c**), and $D = 2 \cdot 10^{-5}\ cm^2/s$ (**d**). The ratchet parameters in **b**, **c**, and **d** are $L = 1\ \mu m$, $x_c = 0.7$, $V_{max} = 2.5\ V$, $\delta = 0.25$, $\alpha = -0.5$. In **c**, and **d** the signal frequency is $f = 83\ kHz$ and the right axis shows the sawtooth potential distribution $U(x,t)$.

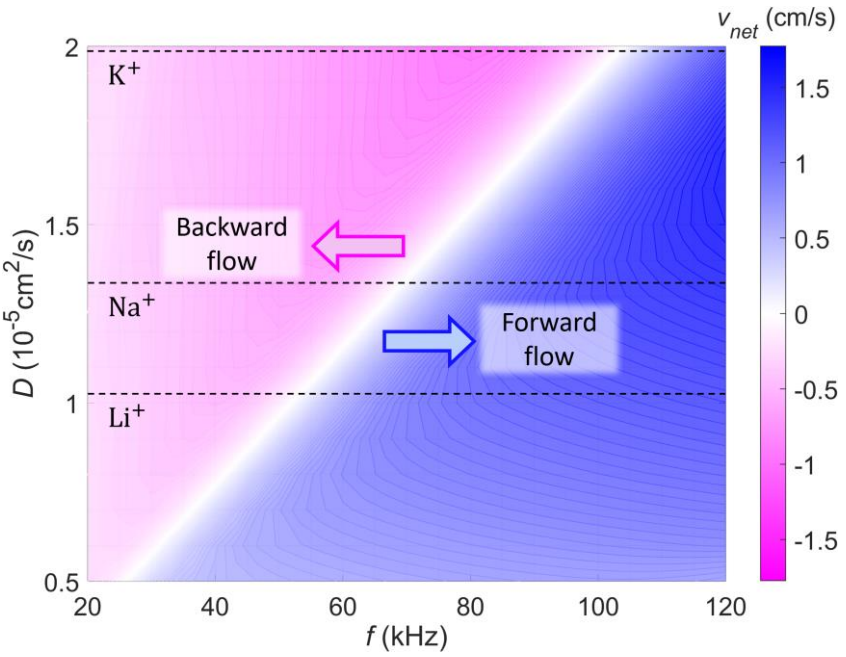

Fig. 3 | Net velocity of monovalent cations as a function of their diffusion coefficient and the signal frequency. All potential and signal parameters are the same as in Fig. 2b-d.

Fig. 3 shows a 2D map of the net velocity of monovalent cations as a function of diffusion coefficient and the input signal frequency. All other ratchet parameters are as in Fig. 2b. It can be easily noticed that the stopping frequency increases with the diffusion coefficient. This implies that for a given frequency, ions with diffusion coefficients above a specific value have a positive velocity, and ions with diffusion coefficients below that value travel in the opposite direction. For example, at a frequency of 60 kHz, Li^+ ($D = 1.03 \cdot 10^{-5}$ cm^2/s) ions travel forwards at a velocity of +0.6 cm/s, but K^+ and Na^+ ($D = 1.96 \cdot 10^{-5}$ and $D = 1.33 \cdot 10^{-5}$ cm^2/s respectively) ions travel backwards with velocities of about –0.8 and –0.5 cm/s respectively. This demonstrates the ability of ratchets to separate ions with the same charge by driving them in opposite directions according to their diffusion coefficients. Moreover, since the input signal determines which ions move forward and which move backward, the ionic selectivity of these ratchets can be tuned in real time.

To analyze the ratchet behavior for a wide range of ratchet parameters, it is useful to normalize the net ion velocity and the signal's frequency by a characteristic ion velocity parameter $v_0 = zD\beta V_{max}/L$ and a characteristic ratchet frequency $f_0 = v_0/L$,[33] respectively. For convenience, a normalized frequency parameter $\Gamma = f/f_0 = fL^2/zD\beta V_{max}$ was also defined. Fig. 4a shows the normalized net ion velocity as a function of Γ with different symmetry factors α. Since the values are normalized, a single curve, that we term the characteristic net velocity curve, contains information about any diffusion coefficient or ratchet period. The inset shows the characteristic net velocity curves in a wider Γ range, illustrating a known ratchet property, that at very low and very high frequencies the output of a ratchet is zero.[33] For moderately low Γ the behavior is similar to the operation shown in Fig. 2d, where the negative net velocity is a result of the injection phenomenon described above.

As α decreases in magnitude, the injection becomes more dominant, and therefore the net velocity becomes more negative. At the moderately high Γ regime, the sign and magnitude of the velocity are determined by the time-averaged potential $\overline{U} = \delta V_{max} + (1-\delta)\alpha V_{max}$. For negative $\overline{U}$ $(\alpha < -0.33)$ the net velocity is positive, and therefore a stopping frequency exists, while for positive $\overline{U}$ $(\alpha > -0.33)$ the net velocity is negative, and there is no stopping frequency, and therefore no velocity reversal. A more detailed analysis of the moderately high normalized frequency regime is given in the SI. Fig. 4b shows the normalized net ion velocity as a function of δ, for $\Gamma = 1$, with different symmetry factors α. As expected, at $\delta = 0{,}1$ there is no net movement of ions since there are no temporal fluctuations. The net velocity is also zero at $\alpha = -1$, $\delta = 0.5$, since the potential distribution is temporally symmetric.[33,43] These 'sine-like' shapes are well known in ratchet systems,[13,27,33] and are a good validation of our model.

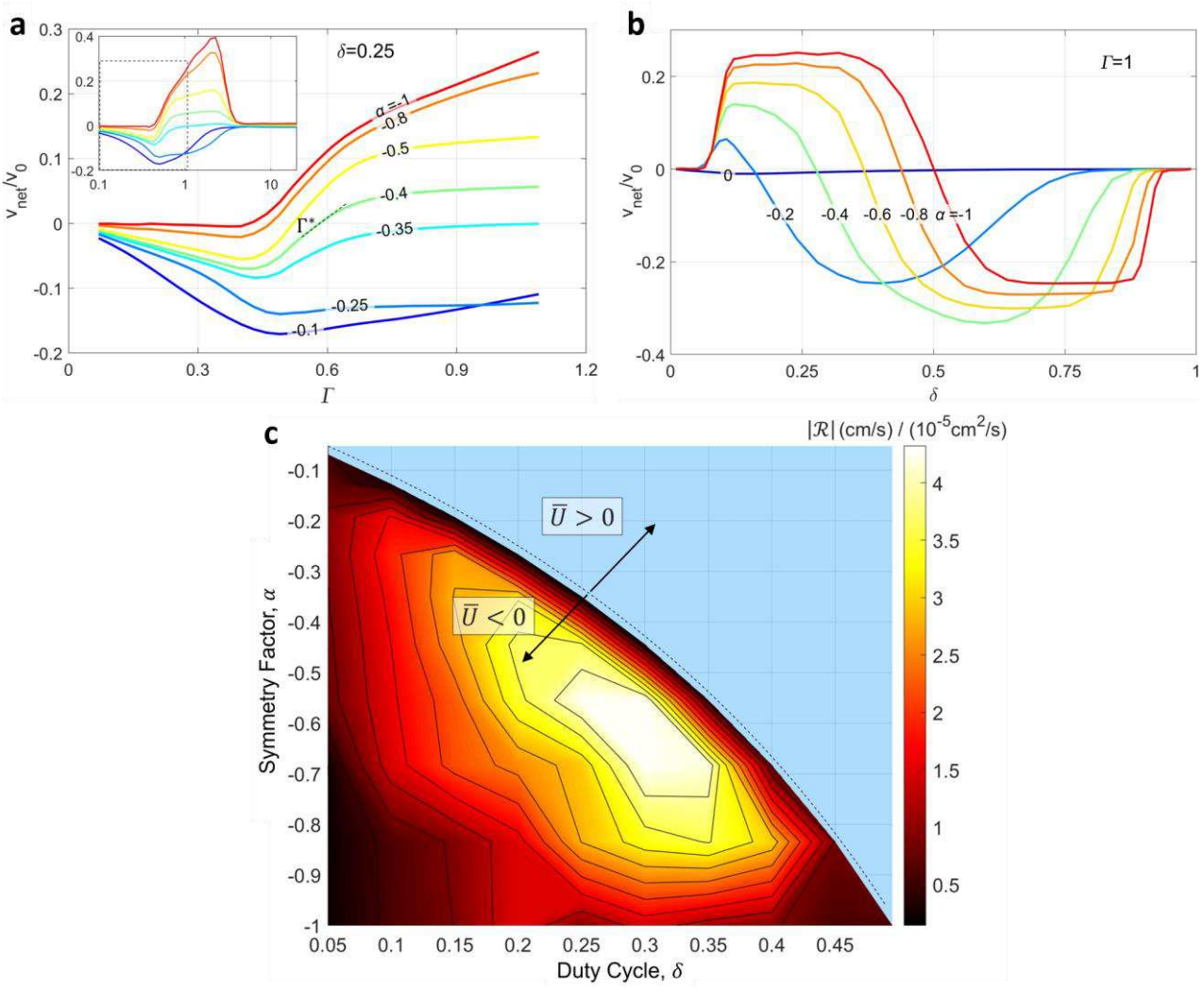

Fig. 4 | Ratchet performance as a function of symmetry factor, α, and duty cycle, δ. a, Characteristic net velocity curves for different symmetry factors α. **b**, Normalized net ion velocity as a function of duty cycle, δ, for different symmetry factors α, and at $\Gamma = 1$. **c,** Separation resolution as function of symmetry factor, α, and duty cycle, δ. In **a**-**c**, unless stated otherwise the ratchet parameters are: $L = 1\ \mu m$, $x_c = 0.7$, $V_{max} = 2.5\ V$, $\delta = 0.25$, $\alpha = -0.5$, and the ion properties are $z = 1$, and $D = 1 \cdot 10^{-5}\ cm^2/s$.

Velocity reversal was shown under the assumption of an infinitely periodic system in which no concentration gradient develops between spatial periods, and hence no work is performed. This is similar to a photovoltaic cell driving current under short circuit conditions where no power is converted. However, when driving ions between two finite reservoirs, an initial concentration gradient can exist, or will develop during operation, which will impede further ion transport. Thus, real systems must separate ions while driving some of the species against a concentration gradient. Frequency controlled velocity reversal in the presence of an ion concentration gradient was demonstrated by simulating a finite ratchet domain, with several spatial periods, operating between two ion reservoirs with varying concentration ratios. The description of the model and the simulation results are given in Supplementary Fig. 3 in the SI. It is shown that velocity reversal is possible even when the ions are transported up a concentration gradient with a concentration ratio as high as 10,000 between two reservoirs. The maximal concentration gradient that the ratchet can overcome increases greatly with the number of the ratchet spatial periods. A more detailed analysis of the ratchet drive against a concentration gradient is left for future work.

The separation resolution

The selectivity of membranes for different same-charge ions is typically expressed in terms of the ratio of fluxes of the desired and undesired species crossing the membrane.[44,45] A highly selective membrane will yield a flux ratio on the order of 100:1 for the wanted species, and typically much lower than that.[45–49] In the case where same-charge ions are transported in opposite directions, and the concentration gradients are small, none of the unwanted ions will cross the membrane, and this selectivity definition ceases to be relevant. Thus, the *separation resolution,* $\mathcal{R}$, is introduced. It is defined as the ability to separate different same-charge ions according to the difference in their diffusion coefficients. According to this definition, a ratchet membrane can separate two types of ions with a diffusion coefficient difference of ΔD, by driving one ion through the membrane at a velocity $v_{net} = \mathcal{R}\Delta D$, while the other ion is kept at its stopping frequency and is not affected by the ratchet. Since this definition describes a linear relation between the difference in diffusion coefficients and the ion net velocity, it becomes less accurate as ΔD increases.

The separation resolution for a certain set of ratchet parameters is calculated according to eq. (6) based on the normalized stopping frequency Γ^*, and the slope of the characteristic net velocity curve $v_{net}/v_0 = \mathcal{H}(\Gamma)$, as shown for example in Fig. 4a (the derivation of eq. (6) is given in the methods section).

$$\mathcal{R}(\alpha, \delta, x_c, \beta V_{max}, L, z) = \left.\frac{\partial v_{net}}{\partial D}\right|_{\Gamma^*} = -\frac{z\beta V_{max}}{L} \cdot \Gamma^* \left.\frac{\partial \mathcal{H}}{\partial \Gamma}\right|_{\Gamma^*} \quad (6)$$

Fig. 4c shows the separation resolution for different symmetry factors, α, and duty-cycles, δ. The light blue region corresponds to input signals that do not yield velocity reversal, showing more

generally that for sawtooth sharpness $x_c > 0.5$, velocity reversal is possible only with $\overline{U} < 0$ (for $x_c < 0.5$ velocity reversal is possible only for $\overline{U} > 0$). High separation resolution is achieved using mid-range symmetry factors ($-0.8 < \alpha < -0.4$,) and mid-range duty-cycles ($0.2 < \delta < 0.4$). The effect of each variable cannot be examined separately because they are interconnected but can be generally understood by referring to eq. (6): (i) Low δ leads to lower Γ^*, since a larger time-period is needed to reach the steady state distribution at $\tau = t^+$. (ii) High α (in magnitude) reduces $\partial\mathcal{H}/\partial\Gamma|_{\Gamma^*}$, due to lower injection. (iii) A combination of high δ and low α (in magnitude) also reduces $\partial\mathcal{H}/\partial\Gamma|_{\Gamma^*}$, since it approaches $\overline{U} = 0$.

The separation resolution is proportional to L^{-1}, therefore low spatial period devices are desired. However, such devices will have to operate at much higher signal frequencies, since the stopping frequency is proportional to L^{-2}. The separation resolution also increases with V_{max}, as shown in Fig. 5a. For lower potential amplitudes the increase is non-linear. This is due to the linear term of V_{max} in eq. (6) and an additional increase of the slope of the characteristic velocity function, $\partial\mathcal{H}/\partial\Gamma|_{\Gamma^*}$, as shown in the inset. For higher values of V_{max} the separation resolution becomes linear with the amplitude reaching $\mathcal{R} = 12\,(\mathrm{cm/s})/(10^{-5}\mathrm{cm^2/s})$ for $V_{max} = 5\,V$. Thus, for two monovalent ions with a difference in diffusion coefficients of $\Delta D = 0.01 \cdot 10^{-5}\ \mathrm{cm^2/s}$, which is a relative difference of about 1% (for the prevalent ions in water), the maximum separation velocity is $\Delta v_{net} = \mathcal{R} \cdot \Delta D = 0.12\ \mathrm{cm/s}$. Fig. 5b and Fig. 5c shows the effect of x_c on the net velocity characteristic curves, and the separation resolution, respectively. As might be expected, when the potential shape is symmetric at $x_c = 0.5$, there is no net ion movement, and the separation resolution is zero. Interestingly, the optimal sawtooth shape for separation is with a moderate asymmetry, $x_c = 0.4$ & 0.6, and as x_c moves towards 0 or 1, the magnitude of $\mathcal{R}$ decrease. A key factor in this behavior has to do with the increase in length of the low field section. Injection requires that ions cross the entire low field section; thus, a longer path for ions to cross implies that injection will occur at a lower normalized frequency. This is apparent in Fig. 5b, where the normalized stopping frequency decrease as the sawtooth becomes more asymmetric, which according to eq. (6), leads to a decrease in the separation resolution. Another interesting feature that can be seen in Fig. 5b is the 'resonance like' behavior of ratchets with moderate spatial asymmetry, such as $x_c = 0.6$. A detailed explanation of this phenomenon is given in the SI, together with an example for a possible application in systems where high selectivity is needed for H^+, such as microbial fuel cells (MFCs)[50] systems. It is shown in Supplementary Fig. 3 that using this 'resonance like' feature, it is possible to achieve a net velocity ratio of 520:1 and 320:1 for H^+ relative to Na^+ and K^+, respectively. Fig. 5d shows the characteristic velocity curves for different ion valence $|z|$, and the separation resolution between same-charge ions as a function of ion valance. The separation resolution increases significantly with $|z|$, due to the linear term in eq. (6), and an increase of the slope $\partial\mathcal{H}/\partial\Gamma|_{\Gamma^*}$. When separating ions with different charge numbers, eq. (6)

cannot be used since different charge numbers result in different characteristic velocity functions. In addition, since drift currents are linear with the ions charge number and diffusion coefficient product, the separation ability is determined by differences in the zD product. Therefore, a case-by-case method should be taken when studying ions with different charge numbers.

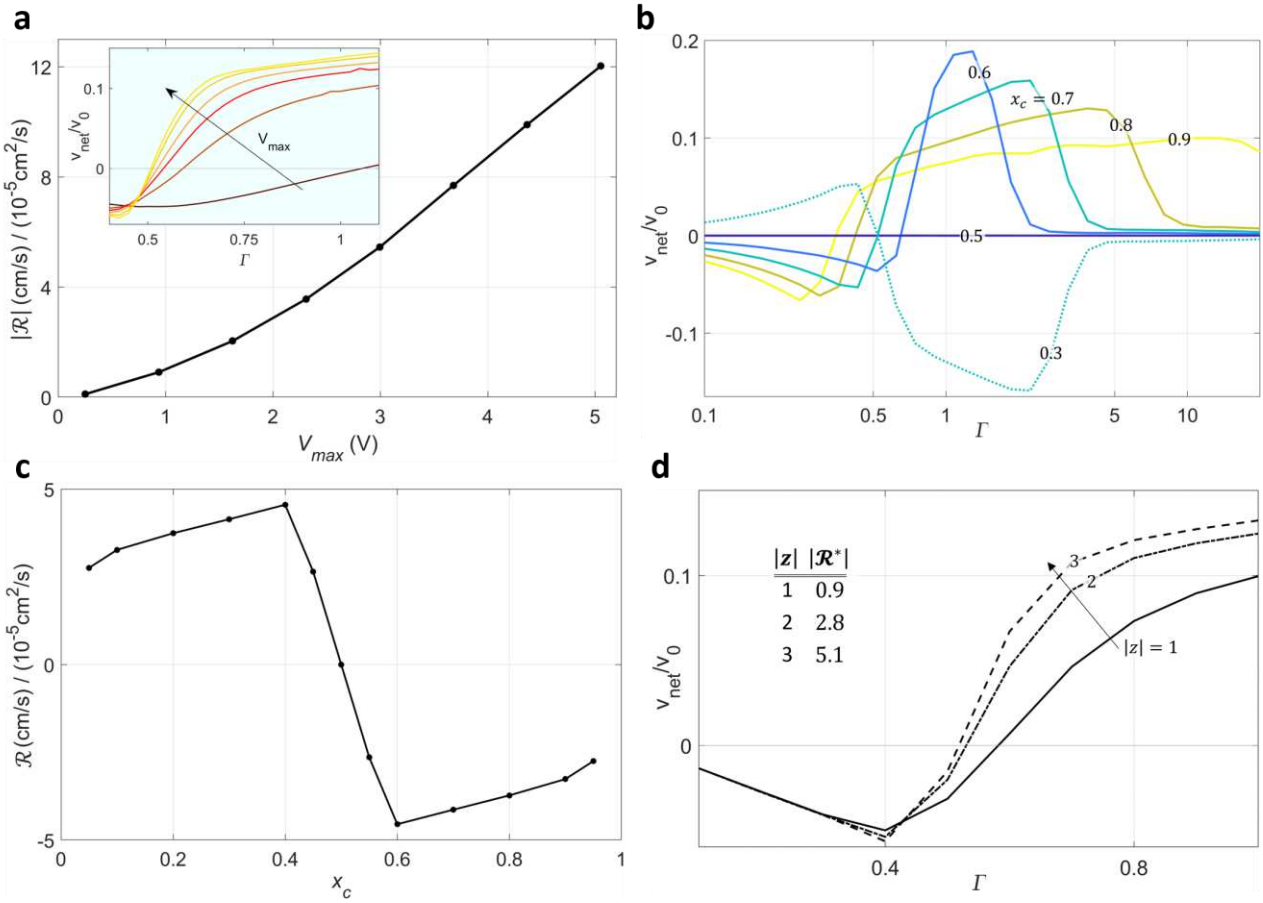

Fig. 5 | Ratchet characteristics as a function of the potential amplitude V_{max}, sawtooth symmetry x_c, and ion valence $|z|$. **a**, Separation resolution magnitude as a function of the maximum amplitude V_{max}. The inset shows the characteristic net velocity curves. **b**, Characteristic net velocity curves for different x_c. **c**, Separation resolution as a function of x_c. **d**, Characteristic net velocity curves for different ion valence $|z|$, with $V_{max} = 1\ V$. The inset table shows the separation resolution between same-charge ions. $|\mathcal{R}^*|$ is in units of $(cm/s)/\ (10^{-5}cm^2/s)$. In **a**-**d**, unless stated otherwise the ratchet parameters are: $L = 1\ \mu m$, $x_c = 0.7$, $V_{max} = 2.5\ V$, $\delta = 0.25$, $\alpha = -0.5$, and the ion properties are $z = 1$, and $D = 1 \cdot 10^{-5}\ cm^2/s$.

Applications and Implications

The unique ability of ratchets to drive particles with the same charge in opposite directions makes them very attractive for ion separation applications. This characteristic may be most significant when targeting the removal of trace ions from a solution where conventional membrane-based separation methods require extreme levels of selectivity. For example, Fig. 6a shows the net velocity as a function of frequency of lead (Pb^{2+}, $zD = 1.89 \cdot 10^{-5}$ cm^2/s), copper (Cu^{2+}, $zD = 1.46 \cdot 10^{-5}$ cm^2/s), lithium (Li^{+}, $zD = 1.03 \cdot 10^{-5}$ cm^2/s), and sodium (Na^{+}, $zD = 1.33 \cdot 10^{-5}$ cm^2/s). Lead can be extracted from contaminated drinking water, with a much higher sodium content, with a

relatively high velocity since they have a high zD difference. However, copper which has a much closer zD value to sodium, cannot be separated from sodium with high velocities, since their stopping frequencies are very close. Lithium is conveniently positioned for extraction from sea water since it has one of the lowest zD values of cations. This means that even though its concentration in the ocean is very low (0.15 ppm),[51,52] it can be separated in a single process from most other cations that are present at much higher concentrations. Another example for the separation of nitrate[45,53] (NO_3^-) and carbonate[44] (CO_3^{2-}) from chloride (Cl^-) is given in Supplementary Fig. 4 in the SI and discussed.

To estimate the performance of a selective ion extraction system, a one-dimensional system was considered, as shown in the inset of Fig. 6b. The system consists of a feed compartment with a width W=1 mm, and two RBIP membranes on its edges (x=±W/2) that extract the ion of interest out of the feed compartment with a constant net ion velocity, termed the extraction velocity. Assuming no convection in the feed compartment, the ion concentration was found by numerically solving the transient diffusion equation with a flux boundary condition at the edges, as described in the methods section. Fig. 6b shows the time required to extract lead ions out of the feed compartment as a function of the extraction velocity. The initial lead ion concentration is 100 ppb, and the extraction time is the time required to extract 99% of lead ions. The inset shows the time evolution of the lead ion distribution in the feed compartment. The extraction velocity is 0.01 cm/s, which is roughly the velocity at which the extraction time saturates. Soon after the extraction begins, the concentration at the edges

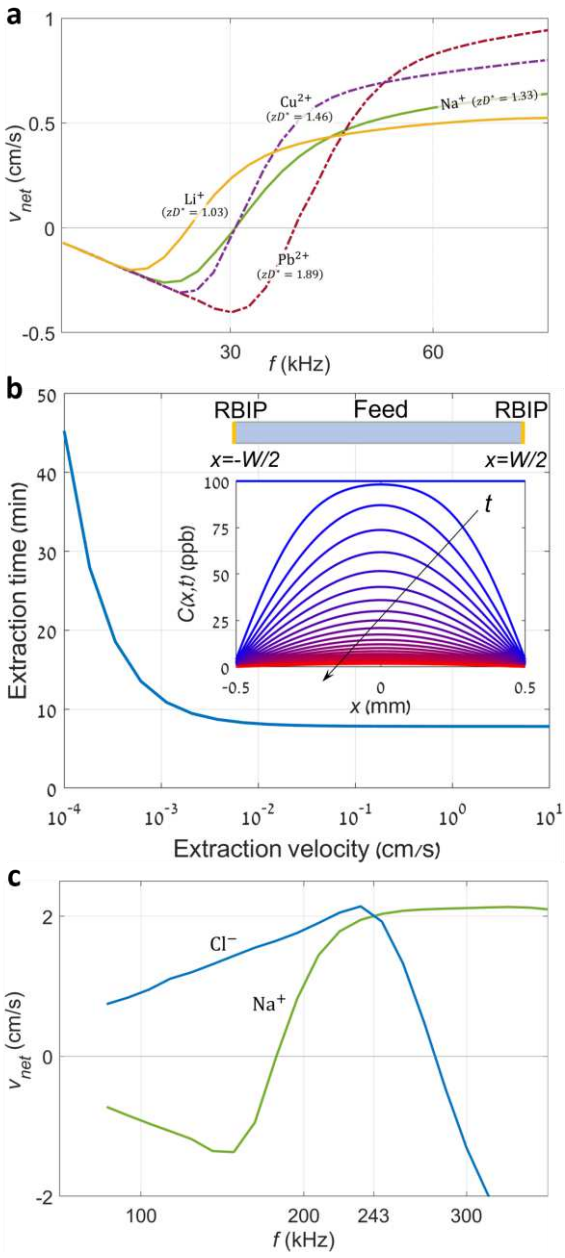

Fig. 6 | Applications and Implications. **a,** Net velocity of Na^+, Li^+, Cu^{2+}, and Pb^{2+} as a function of input signal frequency. The units for zD^* are in $(10^{-5}cm^2/s)$. Ratchet parameters: $L = 1\,\mu m$, $x_c = 0.7$, $V_{max} = 1\,V$, $\alpha = -0.5$, $\delta = 0.25$. **b,** Time to extract 99% of lead ions out of the feed compartment as a function of the extraction velocity. The inset shows the one-dimensional system model, and the time evolution of the lead ion distribution in the feed compartment, using an extraction velocity of 0.01 cm/s. Time step between two adjacent curves is 20 sec. **c,** Net velocity of Cl^- and Na^+ showing ambipolar transport. Ratchet parameters: $L = 1\,\mu m$, $x_c = 0.6$, $V_{max} = 5\,V$, $\alpha = -0.38$, $\delta = 0.25$.

approaches zero, and further extraction is limited by diffusion from the bulk solution. Thus, such systems can be optimal for applications where only a moderate portion of the ions should be removed rapidly. Nevertheless, for systems that are limited by diffusion in the bulk solution, the ratchet induced ion velocity can be as low as 0.01 cm/s without impeding the system performance. The ion extraction time can be decreased substantially by introducing stirring or by reducing the width of the feed compartment to micrometer scale. In such cases ion transport will no longer be limited by bulk diffusion and higher extraction velocities can be utilized.

Velocity reversal can also be used for driving oppositely charged ions in the same direction, a process we term ambipolar ion transport. When both cations and anions are driven in the same direction, there is no charge separation, and therefore an opposing electrostatic potential does not develop, making this an attractive mechanism for desalination applications. Fig. 6c shows an example for ambipolar transport of the main ions in seawater. When the ratchet is operated at 243 kHz, both the negative and positive ions are transported in the same direction at a velocity of 2 cm/s.

Conclusion

In this work we have laid the theoretical groundwork for ratchet-driven ion separation. We have shown that a flashing ratchet can be used to drive ions with the same charge number in opposite directions based on the difference in diffusion coefficients. This unique ratchet property paves the way for rapid extraction of trace ions from solutions where conventional membrane-based separation processes do not offer sufficient selectivity. We define the ratchet separation resolution and show that under moderate voltages, ions with a 1% relative difference in diffusion coefficients can be driven in opposite directions with a velocity difference of 1.2 mm/s. Moreover, non-linearities in the ion velocity with the input signal amplitude and ion valence can be further utilized to enhance the ratchet selectivity. Thus, ratchet-based ion pumping systems may prove beneficial for applications such as water treatment, bio-medical devices, ion sensors, solar fuels generators and more.

Acknowledgments

The authors would like to acknowledge Francesca Toma for helpful discussions. AH acknowledges the support of the Boris Mints Institute. JWA was supported by the Joint Center for Artificial Photosynthesis, a DOE Energy Innovation Hub, supported through the Office of Science of the United States. Department of Energy under Award No. DE-SC0004993. SA acknowledges the support of the Gordon and Betty Moore Foundation under a Moore Inventor Fellowship (GBMF grant #5641) and The Beall Family Foundation (UCI Beall Innovation Award). GS thanks the Azrieli Foundation for financial support within the Azrieli Fellows program.

Conflict of Interest

GS, JWA, and SA filed patent applications US 16/907,076 and US 17/125,341 for ratchet-based ion pumping membrane systems. There are no other conflicts of interest to declare.

Author Contributions

Conceptualization: GS, SA

Investigation: AH, GS

Methodology: AH, JWA, GS

Data curation: AH

Formal analysis: AH

Visualization: AH, GS

Writing – original draft: AH, GS

Writing – review and editing: AH, GS, JWA, SA

Supervision, Project Administration, and Funding Acquisition: GS

References

1. Tang, C. & Bruening, M. L. Ion separations with membranes. *J. Polym. Sci.* **58**, 2831–2856 (2020).
2. Epsztein, R., DuChanois, R. M., Ritt, C. L., Noy, A. & Elimelech, M. Towards single-species selectivity of membranes with subnanometre pores. *Nat. Nanotechnol.* **15**, 426–436 (2020).
3. Sholl, D. S. & Lively, R. P. Seven chemical separations to change the world. *Nature* vol. 532 435–437 (2016).
4. World Health Organization. *Guidelines for drinking-water quality*. (2017).
5. Tang, C., Yaroshchuk, A. & Bruening, M. L. Flow through negatively charged, nanoporous membranes separates Li+and K+due to induced electromigration. *Chem. Commun.* **56**, 10954–10957 (2020).
6. Armstrong, J. A., Bernal, E. E. L., Yaroshchuk, A. & Bruening, M. L. Separation of ions using polyelectrolyte-modified nanoporous track-etched membranes. *Langmuir* **29**, 10287–10296 (2013).
7. Yaroshchuk, A. E. Asymptotic behaviour in the pressure-driven separations of ions of different mobilities in charged porous membranes. *J. Memb. Sci.* **167**, 163–185 (2000).
8. Yaroshchuk, A. E. Dielectric exclusion of ions from membranes. *Advances in Colloid and Interface Science* vol. 85 193–230 (2000).

9. Yaroshchuk, A. E. Negative rejection of ions in pressure-driven membrane processes. *Adv. Colloid Interface Sci.* **139**, 150–173 (2008).

10. Hänggi, P. & Marchesoni, F. Artificial Brownian motors: Controlling transport on the nanoscale. *Rev. Mod. Phys.* **81**, 387–442 (2009).

11. Reimann, P. Brownian motors: Noisy transport far from equilibrium. *Phys. Rep.* **361**, 57–265 (2002).

12. Lau, B. & Kedem, O. Electron ratchets: State of the field and future challenges. *J. Chem. Phys.* **152**, 200901 (2020).

13. Kedem, O., Lau, B. & Weiss, E. A. How to Drive a Flashing Electron Ratchet to Maximize Current. *Nano Lett.* **17**, 5848–5854 (2017).

14. Kedem, O., Lau, B. & Weiss, E. A. Mechanisms of Symmetry Breaking in a Multidimensional Flashing Particle Ratchet. *ACS Nano* **11**, 7148–7155 (2017).

15. Kedem, O., Lau, B., Ratner, M. A. & Weiss, E. A. Light-responsive organic flashing electron ratchet. *Proc. Natl. Acad. Sci.* **114**, 8698–8703 (2017).

16. Tanaka, T., Nakano, Y. & Kasai, S. GaAs-based nanowire devices with multiple asymmetric gates for electrical brownian ratchets. *Jpn. J. Appl. Phys.* **52**, (2013).

17. Linke, H. *et al.* Experimental tunneling ratchets. *Science (80-.).* **286**, 2314–2317 (1999).

18. Mikhnenko, O. V., Collins, S. D. & Nguyen, T. Q. Rectifying electrical noise with an ionic-organic ratchet. *Adv. Mater.* **27**, 2007–2012 (2015).

19. Hu, Y. *et al.* Understanding the Device Physics in Polymer-Based Ionic-Organic Ratchets. *Adv. Mater.* **29**, (2017).

20. Hubmann, S. *et al.* Giant ratchet magneto-photocurrent in graphene lateral superlattices. *Phys. Rev. Res.* **2**, 33186 (2020).

21. Roeling, E. M. *et al.* Organic electronic ratchets doing work. *Nat. Mater.* **10**, 51–55 (2011).

22. Roeling, E. M. *et al.* The performance of organic electronic ratchets. *AIP Adv.* **2**, (2012).

23. Andersson, O., Maas, J., Gelinck, G. & Kemerink, M. Scalable Electronic Ratchet with Over 10% Rectification Efficiency. *Adv. Sci.* **7**, (2020).

24. Olbrich, P. *et al.* Terahertz ratchet effects in graphene with a lateral superlattice. *Phys. Rev. B* **93**, 1–15 (2016).

25. Faltermeier, P. *et al.* Helicity sensitive terahertz radiation detection by dual-grating-gate high electron mobility transistors. *J. Appl. Phys.* **118**, 084301 (2015).

26. Kabir, M., Unluer, D., Li, L., Ghosh, A. W. & Stan, M. R. Electronic Ratchet : A Non-Equilibrium , Low Power. *2011 11th IEEE Int. Conf. Nanotechnol.* 482–486 (2011) doi:10.1109/NANO.2011.6144610.

27. Rozenbaum, V. M. High-temperature brownian motors: Deterministic and stochastic fluctuations of a periodic potential. *JETP Lett.* **88**, 342–346 (2008).

28. Marbach, S. & Bocquet, L. Active sieving across driven nanopores for tunable selectivity. *J. Chem. Phys.* **147**, (2017).

29. Marbach, S., Kavokine, N. & Bocquet, L. Resonant osmosis across active switchable membranes. *J. Chem. Phys.* **152**, (2020).

30. Parrondo, J. M. R., Blanco, J. M., Cao, F. J. & Brito, R. Efficiency of Brownian motors. *Europhys. Lett.* (1998).

31. Nouri, R. & Guan, W. Nanofluidic charged-coupled devices for controlled DNA transport and separation. *Nanotechnology* **32**, 345501 (2021).

32. Ardo, S. *et al.* Ratchet-based ion pumping membrane systems. (2020).

33. Rozenbaum, V. M., Korochkova, T. Y., Chernova, A. A. & Dekhtyar, M. L. Brownian motor with competing spatial and temporal asymmetry of potential energy. *Phys. Rev. E - Stat. Nonlinear, Soft Matter Phys.* **83**, 1–10 (2011).

34. Kodaimati, M. S., Kedem, O., Schatz, G. C. & Weiss, E. A. Empirical Mappings of the Frequency Response of an Electron Ratchet to the Characteristics of the Polymer Transport Layer. *J. Phys. Chem. C* **123**, 22050–22057 (2019).

35. Skaug, M. J., Schwemmer, C., Fringes, S., Rawlings, C. D. & Knoll, A. W. Nanofluidic rocking Brownian motors. *Science (80-.).* **359**, 1505–1508 (2018).

36. Schwemmer, C., Fringes, S., Duerig, U., Ryu, Y. K. & Knoll, A. W. Experimental Observation of Current Reversal in a Rocking Brownian Motor. *Phys. Rev. Lett.* **121**, 104102 (2018).

37. Nicollier, P. *et al.* Nanometer-Scale-Resolution Multichannel Separation of Spherical Particles in a Rocking Ratchet with Increasing Barrier Heights. *Phys. Rev. Appl.* **15**, 034006 (2021).

38. Chen, Q., Ai, B. Q. & Xiong, J. W. Brownian transport of finite size particles in a periodic channel coexisting with an energetic potential. *Chaos* **24**, (2014).

39. Słapik, A., Łuczka, J., Hänggi, P. & Spiechowicz, J. Tunable Mass Separation via Negative Mobility. *Physical Review Letters* vol. 122 (2019).

40. Motz, T., Schmid, G., Hänggi, P., Reguera, D. & Rubí, J. M. Optimizing the performance of the entropic splitter for particle separation. *J. Chem. Phys.* **141**, 074104 (2014).

41. Reguera, D. *et al.* Entropic splitter for particle separation. *Phys. Rev. Lett.* **108**, 1–5 (2012).

42. Yang, B., Long, F. & Mei, D. C. Negative mobility and multiple current reversals induced by colored thermal fluctuation in an asymmetric periodic potential. *Eur. Phys. J. B* **85**, 2–7 (2012).

43. Rozenbaum, V. M., Shapochkina, I. V., Teranishi, Y. & Trakhtenberg, L. I. Symmetry of deterministic ratchets. *Phys. Rev. E* **100**, 22115 (2019).

44. Luo, T., Abdu, S. & Wessling, M. Selectivity of ion exchange membranes: A review. *J. Memb. Sci.* **555**, 429–454 (2018).

45. Sata, T. Studies on anion exchange membranes having permselectivity for specific anions in electrodialysis — effect of hydrophilicity of anion exchange membranes on permselectivity of anions. **167**, 1–31 (2000).

46. Sata, T., Sata, T. & Yang, W. Studies on cation-exchange membranes having permselectivity between cations in electrodialysis. **206**, 31–60 (2002).

47. Luo, T., Roghmans, F. & Wessling, M. Ion mobility and partition determine the counter-ion selectivity of ion exchange membranes. *J. Memb. Sci.* **597**, 117645 (2020).

48. Acar, E. T., Buchsbaum, S. F., Combs, C., Fornasiero, F. & Siwy, Z. S. Biomimetic potassium-selective nanopores. 1–8 (2019).

49. Li, X. *et al.* Fast and selective fluoride ion conduction in sub-1-nanometer metal-organic framework channels. *Nat. Commun.* **10**, 1–12 (2019).

50. Harnisch, F. & Schrçder, U. Selectivity versus Mobility : Separation of Anode and Cathode in Microbial Bioelectrochemical Systems. 921–926 (2009) doi:10.1002/cssc.200900111.

51. Yang, S., Zhang, F., Ding, H. & He, P. Lithium Metal Extraction from Seawater. *Joule* **2**, 1648–1651 (2018).

52. Swain, B. Recovery and recycling of lithium : A review. *Sep. Purif. Technol.* **172**, 388–403 (2017).

53. T. Matos, C., Velizarov, S., G. Crespo, J. o & A.M. Reis, M. Simultaneous removal of perchlorate and nitrate from drinking water using the ion exchange membrane bioreactor c ... bioreactor concept. *water Res.* **40**, (2006).

Methods

Continuity equation computational model

The continuity equation (eq. (1)-(4)) was solved numerically using COMSOL® Multiphysics v5.5. The model domain is $x \in [0, L]$, with a periodic boundary condition defined as $C(0,t) = C(L,t)$, and a normalization condition for the total concentration $\int_0^L C(x,t)dx\,/L = c_0$, where c_0 is a reference ion concentration. The initial condition for the time-dependent simulation was taken as the steady state concentration distribution using the time-averaged potential as an input: $\overline{U}(x) = [\delta + (1-\delta)\alpha]V(x)$. The time-dependent simulation was run over several consecutive temporal periods, until the net ion flux reached a steady state value, and the ratchet operation was independent of its initial condition. The convergence of the net ion flux was not limited by a strict condition, however, typically 4 temporal periods were enough to get a relative difference <1% between the last two periods. The model predictions were validated by comparing them to prior analytical results under similar conditions. See discussion and Supplementary Fig. 1 in the SI.

Detailed calculation of the separation resolution

We would like to find the separation resolution for any set of parameters, represented by a single characteristic net velocity curve $\mathcal{H}(\Gamma)$ and its corresponding normalized stopping frequency Γ^*. Applying the chain rule on the definition of the separation resolution, and remembering at the normalized stopping frequency, $\mathcal{H}(\Gamma^*) = 0$, we obtain:

$$\mathcal{R} = \left.\frac{\partial v_{net}}{\partial D}\right|_{\Gamma^*} = \left.\frac{\partial\left(v_0 \cdot \mathcal{H}(\Gamma)\right)}{\partial D}\right|_{\Gamma^*} = \frac{\partial v_0}{\partial D}\cdot\mathcal{H}(\Gamma^*) + v_0\left.\frac{\partial \mathcal{H}}{\partial D}\right|_{\Gamma^*} = v_0\left.\frac{\partial \mathcal{H}}{\partial \Gamma}\right|_{\Gamma^*}\left.\frac{\partial \Gamma}{\partial D}\right|_{\Gamma^*} \tag{7}$$

Where:

$$\frac{\partial \Gamma}{\partial D} = \frac{\partial}{\partial D}\left(\frac{fL^2}{zD\beta V_{max}}\right) = -\frac{fL^2}{\beta V_{max} zD^2} = -\frac{\Gamma}{D} \tag{8}$$

Inserting into eq. (7) yields:

$$\mathcal{R} = \left(\frac{zD\beta V_{max}}{L}\right)\left(-\frac{\Gamma^*}{D}\right)\cdot\left.\frac{\partial \mathcal{H}}{\partial \Gamma}\right|_{\Gamma^*} = -\frac{z\beta V_{max}}{L}\cdot\Gamma^*\left.\frac{\partial \mathcal{H}}{\partial \Gamma}\right|_{\Gamma^*} \tag{9}$$

Numerical model for the diffusion equation

Assuming no convection, the one-dimensional continuity equation is reduced to the transient diffusion equation:

$$\frac{\partial C(x,t)}{\partial t} = \mathrm{D}\frac{\partial^2 C(x,t)}{\partial^2 x} \tag{10}$$

Eq. (10) was solved numerically within the domain $x \in [0, W/2]$, with the following initial and boundary conditions:

$$C(x,0) = c_0 \tag{11}$$

$$\frac{\partial C}{\partial x}(0,t) = 0 \tag{12}$$

$$N_{ext} = -D\frac{\partial C}{\partial x}\left(\frac{W}{2},t\right) = C\left(\frac{W}{2},t\right)v_{ext} \tag{13}$$

Here, eq. (11) sets a uniform initial concentration in the entire domain, eq. (12) defines symmetry around $x = 0$, and eq. (13) defines the ionic flux at the side of the feed channel, assuming a net ion velocity v_{ext} induced by the RBIP. The numerical analysis was done using the Crank-Nicolson method.[54]

References

54. Cebeci, T. & Bradshaw, P. *Physical and Computational Aspects of Convective Heat Transfer*. (Springer, New York, NY, 1988). doi:10.1007/978-1-4612-3918-5_13.

Supplementary Files

This is a list of supplementary files associated with this preprint. Click to download.

- RatchetbasedionpumpsforselectiveionseparationsSInofields.pdf